Pion double charge exchange on nickel isotopes and generalized seniority

D. R. Benton, H. T. Fortune, J. M. O'Donnell, R. Crittenden, M. McKinzie,
E. Insko, R. Ivie, D. Smith, and J. D. Silk
Physics Department, University of Pennsylvania, Philadelphia, Pennsylvania 19104
(Received 7 August 1991)

Forward angle ($\theta_{lab} = 5°$) differential cross sections for pion double charge exchange (π^+, π^-) on ^{60}Ni, ^{62}Ni, ^{64}Ni, and ^{nat}Ni have been measured at a π^+ kinetic energy of 293.4 MeV for reactions resulting in the double isobaric analog states. These cross sections are compared with the general trends seen in other double-charge-exchange reactions and with a generalized seniority model based on a sequential reaction mechanism. Results for nonanalog reactions involving the residual Zn ground states are also presented.

PACS number(s): 25.80.Gn

I. INTRODUCTION

Pion double charge exchange (DCX) resulting in either the double isobaric analog state (DIAS) or nonanalog states has generated a great deal of interest [1]. At pion kinetic energies of 150–300 MeV, forward angle cross sections for the analog reactions roughly follow an $A_{tgt}^{-10/3}$ mass dependence [2], though data for targets with isospin $T = 1$ and $T > 1$ exhibit different mass behavior [3]. To explain the finer points of the data, however, requires a good knowledge of the nuclear structure of the nuclei involved in the reaction. For most target nuclei in the medium to heavy mass region, this knowledge is imperfectly known.

The simplest way to proceed would be to make measurements on a set of different nuclei which differ only in the number of nucleons in the same active shell. For even further simplification, one would prefer target nuclei with only one type of active nucleon — either protons or neutrons. The Ni isotopes are nearly ideal for these criteria. Though of higher mass than the Ca isotopes (and therefore smaller cross sections by the $A_{tgt}^{-10/3}$ rule), they consist of a core $N = Z = 28$, with differing number of valence neutrons. Four of the even Ni isotopes can be made as targets. The active shell-model space consists of three ($p_{3/2}$, $p_{1/2}$, $f_{5/2}$) nearly degenerate shells. The DIAS cross section at 5° and $\approx$ 292 MeV has been measured previously only for ^{58}Ni [4, 5]. In this paper we present results for the other even, naturally occurring isotopes of nickel.

The model which we will compare to the data was originally presented by Auerbach, Gibbs, and Piasetzky [6] for the Ca isotopes, but later expanded by Auerbach, Gibbs, Ginocchio, and Kaufmann (AGGK) [7] to include both protons and neutrons in the active shell. This model is based on a sequential reaction mechanism and good seniority or good generalized seniority. All DIAS cross sections can be expressed in terms of three parameters, which can depend on the laboratory scattering angle (θ_{lab}) and incident pion kinetic energy (T_π), but not on N, Z, or A_{tgt} (except through a known A_{tgt} dependent distortion factor).

Using the Ni isotopes in a DCX measurement should, then, provide a data set against which candidates for models can be compared, with minimal complications arising from lack of knowledge of the nuclear structure. The availability of four Ni isotopes constrains the three parameters in the Auerbach *et al.* model, and the Ni isotopes should also give the closest approximation to the assumptions of the generalized seniority model mentioned above.

At 292 MeV, DIAS (and, to a limited extent, ground-state) cross sections have been compared to the $f_{7/2}$ version of the AGGK model in Refs. [4,7]. Data at low energies, primarily 35 and 50 MeV, have also been fitted to the $f_{7/2}$ model [7–11]. The more general version [7] of AGGK allows expressions for DIAS and ground-state cross sections in a space containing several degenerate orbitals, assuming generalized seniority.

II. THE EXPERIMENT AND DATA ANALYSIS

The Energetic Pion Channel Spectrometer (EPICS) at the Clinton P. Anderson Meson Physics Facility (LAMPF) was used for this experiment. The channel provided pions with kinetic energy of 293.4 MeV. The nickel targets used were a set of isotopically enriched Ni foils along with a natural Ni target. The isotopic targets were all placed in the same target frame, the strip from which each detected pion came being found by flight path reconstruction. The thicknesses of the targets are given in Table I. A set of CH_2 targets with the same shapes and placed in the same positions as the Ni targets was used for data normalization. The spectrometer was set at 5° in the laboratory frame for the Ni DCX runs and at 35° for the CH_2 elastic runs.

Muon rejection was accomplished by a plastic scintillator placed at the end of the spectrometer after an amount of aluminum, graphite, and plastic adequate to stop pions and electrons passing through the spectrometer. Reconstructed target position cuts were applied to the data not only to identify the target in which the reaction took place but also to reject extraneous events. Only events with spectrometer time-of-flight values corresponding to

TABLE I. Targets used in the present measurements at 293.4 MeV.

Type	Area (cm^2)	Areal density (g/cm^2)	Purity %
^{60}Ni	37.5	0.151	99.07
^{62}Ni	22.5	0.295	96.72
^{64}Ni	37.5	0.146	97.93
^{nat}Ni[a]	157.5	1.585	99.2
CH_2	See above	0.0238	

[a]For the full natural target, two pieces of this size were used.

pions were kept for final analysis. The Čerenkov detector usually used at EPICS was found to be inoperable during these measurements, and so was not used in the analysis. Because of the relatively large cross sections (for DCX) of the DIAS at these energies, this problem did not appreciably affect the quality of the data. The spectrometer acceptance as a function of focal plane position and target position was derived from π^+ elastic scattering measurements from ^{12}C. The data were also corrected for chamber efficiency, computer livetime, and pion survival fraction. A beam current monitor in the region of the pion production target was used for data normalization.

Replayed data from each target (each of the Ni and CH_2 targets), after the cuts given above, were binned into histograms as a function of reaction Q value. These histograms were then fitted with the sum of a Gaussian and exponential tail (for the DIAS peak) and a cubic polynomial (for the background). The background contribution to the area of the peak ranged from about 5 to 25 percent for the Ni DCX data and was negligible for the H elastic scattering data. It comes mostly from misidentified electrons which have made it through the spectrometer. The time-of-flight parameter did not have enough precision to differentiate between electrons and pions at these high energies. As the Gaussian and exponential form did not always accurately reproduce the actual elastic peak shape, only the background polynomial from the aforementioned fit was used. This background was subtracted from the normalized and corrected counts, the result being summed in the region of the DIAS peak. The summed value from each of the Ni targets was normalized to the summed value in the hydrogen elastic peak from the corresponding CH_2 target position. The H elastic scattering cross section at $\theta_{lab} = 35°$ and $T_\pi = 293.4$ MeV, was taken to be 16.43 mb/sr [12].

We have paid careful attention to the possibility of the dependence of extracted DIAS cross sections on the fitting procedure. The procedure discussed above was checked by comparing results with fitting to a Gaussian with exponential tail shape and fitting to the measured elastic peak shape. Differences between the results of these methods are much smaller than the statistical errors. Uncertainty in the background level has negligible effect on the cross sections obtained from the isotopic targets, but does add an additional uncertainty to the DIAS cross section from the natural Ni target, which has been included in the errors quoted here.

Histograms for the Ni targets are shown in Fig. 1. The

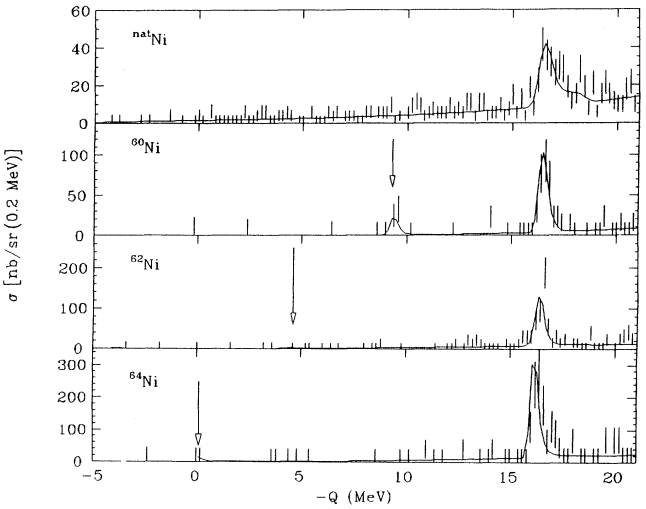

FIG. 1. Q-value histograms of DCX on the isotopic and natural Ni targets. Statistical error bars are included. The arrows indicate the ground-state Q values. The solid lines represent the background and elastic peak shape fits. The vertical scales are in nb/sr(0.2 MeV).

errors given are statistical. The vertical axes are numbered in normalized counts per Q-value bin. The solid line in each figure shows the sum of the background shape and the elastic peak shape which was fitted to the spectra. The vertical arrows show the positions of the appropriate Zn ground states. The ground-state cross sections were also extracted, though they are much smaller than the DIAS cross sections. As the main objective of this experiment was to measure the DIAS cross sections, the spectrometer was set to optimize the efficiency for detecting those events, to the detriment of the ground-state reaction counting rate. These two situations conspired to give the result that there were only a few events per target measured for the ground-state reactions. Because of the limited number of counts in the ground-state peaks, we have simply summed counts. However for ^{60}Ni we plot elastic line shape fits for both the DIAS and the ground states in Fig. 1.

The presence of the natural Ni target in this experiment allows an estimate of the contribution of electrons to the background because this target is significantly thicker than the isotopic targets, and because it is mostly composed of ^{58}Ni for which the DIAS is the ground state, and below which there can be no real pion events. Using the fact that the electron rate increases roughly as the square of the target thickness, and comparing the background rate for the natural and isotopic targets allows the background to be decomposed into a pion contribution and electron contribution. For this decomposition we have assumed that the electron rate is roughly independent of neutron number. Table II shows the results of this decomposition in terms of cross sections integrated over an energy range of the same width as the ground-state peaks. These values have been calculated by summing over three 5 MeV regions for each isotope taken from Q-value regions 8 to 3 MeV, 3 to −2 MeV, −2 to −7 MeV, and −7 to −12 MeV, depending upon the lo-

TABLE II. Decomposition of pion and electron backgrounds for isotopic targets.

σbackground (nb/sr MeV)	$A_{tgt} = 60$	$A_{tgt} = 62$	$A_{tgt} = 64$
σ^e below g.s.	2.7 ± 0.5	2.4 ± 0.7	0.3 ± 0.2
σ^e at g.s.	3.9 ± 0.6	5.1 ± 0.9	1.2 ± 0.3
σ^e above g.s.		7.4 ± 1.2	2.4 ± 0.4
σ^π below g.s.	1.1 ± 2.7	2.6 ± 3.0	-0.3 ± 0.2
σ^π at g.s.	-0.6 ± 6.9	5.9 ± 4.8	3.4 ± 9.6
σ^π above g.s.		4.8 ± 4.5	17.9 ± 9.1

cation of the ground state. Then the resultant number was scaled to give the background cross section for a 1 MeV interval. The region between the ^{60}Ni ground state and DIAS was considered to be too narrow to use this procedure. Table II gives the cross sections for both pions and electrons at Q values below the ground state, at the position of (but not including) the ground state, and between the ground state and the DIAS. As can be seen from these values, the pion contribution below the ground state is obviously consistent with zero, but does have some contribution between the ground state and the DIAS. The only ground-state cross section for which the background could contribute significantly to the sum is σ_{62}, because of the larger target thickness and the small size of the cross section. These background values have been subtracted from the ground-state cross sections and errors adjusted accordingly.

The Q values for DCX resulting in the DIAS were around 16.4 MeV for all isotopes and are given in Table III. The cross section for ^{58}Ni has been calculated from the ^{nat}Ni target with cross sections for the other naturally occurring Ni isotopes subtracted off. These values are given in Table III. The ground-state cross sections are also included in the table.

The value of the cross section at $A_{tgt} = 58$ used in the following section is 121 ± 15 nb/sr, which is the weighted average of the previously published values of 110 ± 17 nb/sr [5] and 152 ± 28 nb/sr [4]. Note that the value obtained in the present measurement from the ^{nat}Ni cross section (134 ± 44 nb/sr) is consistent with this average. Alternatively, one could use the ^{nat}Ni cross section and the previous value for ^{58}Ni to find an additional ^{60}Ni value. This is 328 ± 108 nb/sr compared with the 295 ± 55 nb/sr value obtained from the isotopic target.

TABLE III. Differential cross sections of DCX for DIAS and ground-state transitions on $^{A_{tgt}}$Ni and associated Q values.

A_{tgt}	Q_{DIAS} [c] (MeV)	σ_{DIAS} (nb/sr)	$Q_{g.s.}$ [d] (MeV)	$\sigma_{g.s.}$ (nb/sr)
58[a]		121 ± 15		
60	16.42±0.03	295 ± 55	9.3	61 ± 23
62	16.24±0.03	471 ± 72	4.6	3 ± 9
64	16.19±0.03	974 ± 172	0.1	41 ± 30
nat[b]	16.46±0.04	198 ± 26		

[a]Value from previous data [5, 4], see text.
[b]Full target occupying all of target frame.
[c]Measured here.
[d]Computed from previously measured masses.

III. COMPARISON WITH MODELS

The data from this experiment are plotted in Fig. 2. Also shown in Fig. 2(a) is a dashed curve given by the equation

$$\sigma_{A_{tgt}} = 68 \text{ nb/sr}(N - Z)(N - Z - 1)\left(\frac{A_{tgt}}{42}\right)^{-3.24} \quad (1)$$

(A_{tgt} is the target atomic mass, N is the target neutron number, and Z is the target atomic number), which is the result of a fit to previous DCX DIAS data at ≈ 292 MeV [2] (dashed line). This curve has $\chi^2 = 24.4$. The $A_{tgt} = 58$ point alone has $\chi^2 = 23.8$. Quite clearly, expression (1) cannot account for both $T = 1$ and $T > 1$ data. As the mass dependence has been averaged over many different nuclei without regard for nuclear structure, it should not be expected to reproduce the changes that occur when neutrons are successively added to a single shell.

As mentioned in the Introduction, a model of sequential DCX reactions using generalized seniority has been put forward by Auerbach, Gibbs, Ginocchio, and Kaufmann [7] (AGGK). This model has the virtue of express-

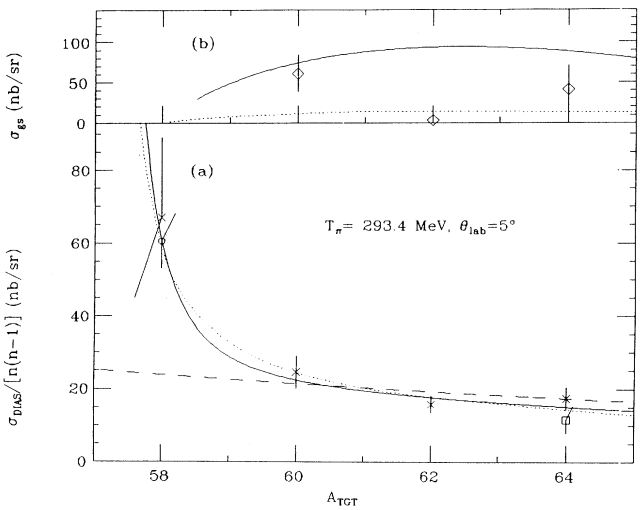

FIG. 2. DCX differential cross sections measured in this experiment in nb/sr for the different Ni isotopes for the (a) DIAS transitions [divided by $n(n-1)$] and (b) the reaction resulting in the Zn ground states. Error bars are statistical. The dashed curve in (a) uses the mass dependence from Ref. [2]. The circular point at $A_{tgt} = 58$ is the weighted average of previous data [4, 5]. The square point at $A_{tgt} = 64$ is calculated from the cross sections for 58, 60, and 62 using Eq. (3) in the text. The solid curves are the results of a fit of the three-parameter seniority-zero model of AGGK [7], with mass distortions taken into account, to the DIAS data only. The dotted curves result from a fit using both the DIAS data and the nonanalog data. The dotted line in (b) is one-half of the predicted result with the new parameters.

ing cross sections in terms of only a few parameters, but also the drawback that because generalized seniority has been assumed, this model is not expected to apply to nuclei in general. However, the Ni isotopes should be one of the best systems for applying it, because the valence nucleons of the target are all of the same type and the active orbitals are nearly degenerate. For this case the expression for the cross section is

$$\sigma_{\rm DIAS} = \frac{n(n-1)}{2}\left|A + \frac{\Omega+1-n}{(\Omega-1)(n-1)}B\right|^2, \qquad (2)$$

where n is the number of valence nucleons (for Ni this is $A_{\rm tgt} - 56$), Ω is the number of valence nucleons required to fill half of the shell (= 6 for Ni), and A and B are complex parameters of the model, giving a total of three free parameters. For little or no spin dependence, A corresponds to the long-range part of the reaction and B to the short-range part. The quantities A and B are independent of N and Z, but dependent on $\theta_{\rm lab}$ and T_π. In addition, $|A|$ and $|B|$ depend on $A_{\rm tgt}$ only through distortions as shown in Fig. 6 of AGGK (note, however, that the labels of A and B are interchanged). As can be seen from the values of $(\Omega+1-n)/(\Omega-1)/(n-1)$ for each isotope (see Table IV), the value of A dominates the cross section for target isospin $T > 1$ ($A_{\rm tgt} > 58$), while for ^{58}Ni the values of A and B contribute roughly equally.

The solid line in Fig. 2(a) is the result of a weighted least-squares fit of this equation to the present DIAS data, varying the magnitude of A and B and the phase between them. A mass dependence of the cross sections in the form $A_{\rm tgt}^{-4.04}$ (Ref. [7]) has been taken out prior to the fitting. The result of the fit is that for $A_{\rm tgt} = 60$, $|A| = 6.29 \pm 0.25\,({\rm nb/sr})^{1/2}$, $|B| = 7.08 \pm 0.68\,({\rm nb/sr})^{1/2}$, with the phase difference between them, $\phi = 79° \pm 7°$. The fit has $\chi^2 = 1.45$.

Another way of doing the same thing is to use three of the cross sections to predict a fourth, because there are three parameters in the model. To predict the ^{64}Ni cross section from the other three, the formula is

$$\sigma_{64} = \frac{4\sigma_{58} - 18\sigma_{60} + 20\sigma_{62}}{7}, \qquad (3)$$

where the coefficient of σ_{60} has been corrected from the AGGK paper. In this procedure, the mass dependence, $A_{\rm tgt}^{-4.04}$, has been taken out as done previously. Using the present data of σ_{58}, σ_{60}, and σ_{62} gives a value of 646 ± 211 nb/sr for σ_{64}. The measured point lies near the limit of the error bar of this derived value.

In addition to the DIAS cross sections, the nonanalog cross sections can also be predicted from the A and B coefficients in the AGGK seniority formalism. For the initial and final nuclei with $J^\pi = 0^+$, and for a target nucleus having total isospin, $T = n/2$, going to $T' = T - 2$, the cross section is given by

$$\sigma_{\rm g.s.} = \frac{n\Omega^2(n-2)(2\Omega+2-n)(2\Omega+1)}{2(\Omega-1)^2(2\Omega+1)^2(n-1)}|B|^2. \qquad (4)$$

Here B, n, and Ω are the same as in Eq. (2). Using this formula (with mass distortions), and the value of $|B|$ given above, gives the predicted ground-state cross sections in Table IV. The ground-state cross sections are plotted in Fig. 2(b) along with a solid line computed using Eq. (4) and $|B|$ from the fit to the DIAS. Adding the ground-state data without changing the model parameters gives a new $\chi^2 = 118$ ($\chi^2/\nu = 29.5$), which is clearly inconsistent. Auerbach *et al.* pointed out that the nonanalog cross sections predicted by this simple model are reduced by approximately a factor of 2 if realistic wave functions are used for the initial and final states [7]. Dividing the predicted nonanalog cross sections by 2 gives $\chi^2 = 26.3$ ($\chi^2/\nu = 6.6$), still not consistent with the ground-state data.

Doing a simultaneous fit to the DIAS and ground-state data (with predicted nonanalog cross sections divided by 2) gives the parameters $|A| = 6.2 \pm 0.3\,({\rm nb/sr})^{1/2}$, $|B| = 3.9 \pm 0.6\,({\rm nb/sr})^{1/2}$, $\phi = 50° \pm 40°$, and $\chi^2 = 8.7$ ($\chi^2/\nu = 2.2$). This fit is shown in both Figs. 2(a) and (b) as a dotted line. Forcing ϕ to be exactly zero gives $|A| = 6.18 \pm 0.27({\rm nb/sr})^{1/2}$ and $|B| = 4.04 \pm 0.50({\rm nb/sr})^{1/2}$ with

TABLE IV. Fit of experimental DCX differential cross sections to AGGK model and results of calculations. Data have been multiplied by a factor $(A_{\rm tgt}/60)^{4.04}$ before fitting.

$A_{\rm tgt}$	n	Model	$\sigma^{\rm expt}$ (nb/sr)	$\sigma^{\rm calc}$ (nb/sr)[a]	$\sigma^{\rm calc}$ (nb/sr)[b]
58 DIAS	2	$\lvert A+B\rvert^2$	121 ± 15	121	117
60 DIAS	4	$6\lvert A+\frac{1}{5}B\rvert^2$	295 ± 55	269	293
62 DIAS	6	$15\lvert A+\frac{1}{25}B\rvert^2$	471 ± 72	529	532
64 DIAS	8	$28\lvert A-\frac{1}{35}B\rvert^2$	974 ± 172	843	801
60 g.s.	4	$1.477\lvert B\rvert^2$	65 ± 23	74	11
62 g.s.	6	$2.127\lvert B\rvert^2$	8 ± 8	93	14
64 g.s.	8	$2.279\lvert B\rvert^2$	42 ± 30	88	13

[a]This fit does not include the nonanalog data. The resultant parameters are $|A| = 6.29 \pm 0.25$, $|B| = 7.08 \pm 0.68$ [both in $({\rm nb/sr})^{1/2}$]. $\phi = 79° \pm 7°$, and $\chi^2 = 1.45$ (with same parameters but including nonanalog data, $\chi^2 = 26.3$, dividing nonanalog model results by 2).

[b]This fit includes both DIAS and nonanalog data. The calculated ground-state values are assumed to be half of the result of expression (4). The fit parameters are $|A| = 6.2 \pm 0.3$, $|B| = 3.9 \pm 0.6$, $\phi = 5° \pm 40°$, and $\chi^2 = 8.7$.

TABLE V. Comparison of AGGK model [7] parameters obtained for $1f_{7/2}$ orbital and for the data presented here. Fits for Ca data have been done identically to those for Ni data [including the mass distortion factor $(A_{\rm tgt}/60)^{4.04}$ multiplied to the data]. The parameter values are in $({\rm nb/sr})^{1/2}$.

	$\|A\|$	$\|B\|$	ϕ (deg)	χ^2/ν
Ca[a] DIAS only	5.1	7.4	79	
Ni DIAS only	6.3 ± 0.3	7.1 ± 0.7	79 ± 7	1.5
Ca[a] DIAS + g.s.	5.4 ± 0.3	3.3 ± 0.5	0 ± 38	2.2
Ni DIAS + g.s.	6.2 ± 0.3	3.9 ± 0.6	5 ± 40	2.2

[a] ^{42,44,48}Ca DIAS and ground-state data from Refs. [4,9].

χ^2 virtually identical to the case where ϕ was allowed to vary.

These procedures demonstrate that though the AGGK model is adequate in fitting the DIAS data, it does not do well with nonanalog cross sections. In particular it does not reproduce the suppression of cross section which seems to occur at midshell (^{62}Ni).

The values of A and B obtained in the present experiment are relevant within the $(1f_{5/2}, 2p_{3/2}, 1p_{1/2})$ series of orbitals, whereas those of Ref. [7] are for the $1f_{7/2}$ orbital only. However a fit to ^{42,44,48}Ca DCX data can be instructive. The results of such a fit to ≈ 292 MeV DCX data at 5° [4, 13] are given in Table V. The coefficients turn out to have similar values as for the Ni data. Doing a simultaneous fit of the Ni and Ca DIAS data and varying not only $|A|$, $|B|$, and ϕ, but also the exponent involved in correcting for the mass distortions results in $|A| = 5.98 \pm 0.14\,({\rm nb/sr})^{1/2}$, $|B| = 6.72 \pm 0.39\,({\rm nb/sr})^{1/2}$, $\phi = 64° \pm 5°$, and a factor of $(A_{\rm tgt}/60)^{3.17 \pm 0.21}$ applied to correct for mass distortions. This fit has $\chi^2 = 2.63$ or $\chi^2/\nu = 0.88$. Of course A, B, and ϕ are not really free parameters, but can in principle be calculated in a full distorted wave description of the DCX process, in which microscopic wave functions are used. At present, outputs of such attempts at realistic calculations resemble parameters obtained from fitting data, but provide poorer agreement with measured cross sections.

IV. SUMMARY

Differential DIAS DCX cross sections have been measured for a variety of Ni isotopes at $T_\pi = 293.4$ MeV and $\theta_{\rm lab} = 5°$. The cross sections lie close to the mass dependence curve of $\sigma_{A_{\rm tgt}} \sim (N - Z)(N - Z - 1)\,(A_{\rm tgt})^{-10/3}$ (except for the $T = 1$ case of ^{58}Ni). The model of AGGK [7] fits well to the present DIAS data with one degree of freedom, but fails to adequately reproduce the ground-state cross sections.

ACKNOWLEDGMENTS

This work was supported by the National Science Foundation. We thank N. Auerbach, W. R. Gibbs, and J. N. Ginocchio for useful discussions.

[1] C. L. Morris *et al.*, Phys. Rev. C **25**, 3218 (1982); S. J. Greene *et al.*, *ibid.* **25**, 927 (1982); Mikkel B. Johnson, *ibid.* **22**, 192 (1980).
[2] R. Gilman *et al.*, Phys. Rev. C **35**, 1334 (1987).
[3] P. Seidl *et al.*, Phys. Rev. C **30**, 973 (1984).
[4] J. D. Zumbro *et al.*, Phys. Rev. C **36**, 1479 (1987).
[5] K. K. Seth *et al.*, Phys. Lett. **173B**, 397 (1986).
[6] N. Auerbach, W. R. Gibbs, and E. Piasetzky, Phys. Rev. Lett. **59**, 1076 (1987).
[7] N. Auerbach *et al.*, Phys. Rev. C **38**, 1277 (1988).
[8] K. K. Seth, Nucl. Phys. **A478**, 591c (1988).
[9] Z. Weinfeld *et al.*, Phys. Rev. C **37**, 902 (1988).
[10] Z. Weinfeld *et al.*, Phys. Lett. B **237**, 33 (1990).
[11] H. W. Baer *et al.*, Phys. Rev. C **43**, 1458 (1991).
[12] Phase shifts taken from G. Rowe, M. Salomon, and R. H. Landau, Phys. Rev. C **18**, 584 (1978).
[13] M. Kaletka *et al.*, Phys. Lett. B **199**, 336 (1987).